# Modeling of Inter-Filament Coupling Currents and Their Effect on Magnet Quench Protection

E. Ravaioli, B. Auchmann, G. Chlachidze, M. Maciejewski, GL. Sabbi, S.E. Stoynev, and A. Verweij

***Abstract*—Variations in the transport current of a superconducting magnet cause several types of transitory losses. Due to its relatively short time constant, usually of the order of a few tens of milliseconds, inter-filament coupling loss can have a significant effect on the coil protection against overheating after a quench. This loss is deposited in the strands and can facilitate a more homogeneous transition to the normal state of the coil turns. Furthermore, the presence of local inter-filament coupling currents reduces the magnet's differential inductance, which in turn provokes a faster discharge of the transport current. The Lumped-Element Dynamic Electro-Thermal (LEDET) model of a superconducting magnet has been developed to reproduce these effects. Simulations are compared to experimental electrical transients and found in good agreement. After its validation, the model can be used for predicting the performance of quench protection systems based on energy extraction, quench heaters, the newly developed CLIQ protection system, or combinations of those. The impact of inter-filament coupling loss on each protection system is discussed.**

***Index Terms*—accelerator magnet, AC loss, modeling, quench protection, superconducting coil.**

## I. Introduction

TRANSITORY losses develop in superconducting wires and cables subject to magnetic-field variations [1]–[4]. The most common loss contributions include inter-filament and inter-strand coupling losses, hysteresis loss, and eddy currents. Transitory losses are a source of local heat generation, non-linear frequency-dependent variations of the superconducting coils' impedances, and magnetic-field errors.

Furthermore, transitory losses have a twofold effect on the magnet discharge. First, they change the magnet's differential inductance [5]–[8]. In fact, in an ideal inductor the local magnetic flux linked in the coil $\Phi$ [Wb] is proportional to the magnet transport current $I_\mathrm{m}$ [A] and its self-inductance is constant. Losses, which affect the local magnetic field, prevent $\Phi$ from changing linearly with $I_\mathrm{m}$. Thus, they influence the effective differential self-inductance of the magnet, $L_\mathrm{d}$=$d\Phi/dI_\mathrm{m}$ [H]. Second, they generate heat in the superconductor, which facilitates the transition of coil sections to the normal state and the consequent increase of the coil resistance. A transition of a superconducting coil to the normal state induced by transitory losses is sometimes referred to as quench back [9]–[12].

Work supported by the US Department of Energy through the US LHC Accelerator Research Program (LARP) and by the High Luminosity LHC Project at CERN.

E. Ravaioli and GL. Sabbi are with the Lawrence Berkeley National Laboratory, Berkeley, CA. (e-mail: ERavaioli@lbl.gov).

G. Chlachidze and S.E. Stoynev are with Fermi National Accelerator Laboratory, Batavia, IL.

B. Auchmann and A.P. Verweij are with CERN, Switzerland.

M. Maciejewski is with CERN, Switzerland, and with Institute of Automatic Control, Technical University of Łódź, 18/22 Stefanowskiego St., Poland.

Manuscript received September 6, 2016.

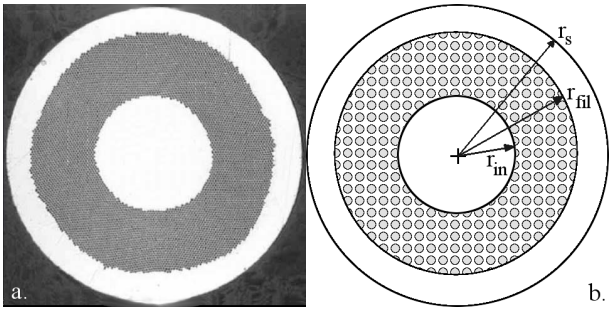


Fig. 1. Cross-section of the strand used in the cable of the outer layer of the LHC main dipole magnets [18]. a. Photography. b. Schematic representation [7].

Due to its relatively short time constant, typically of the order of a few milliseconds or tens of milliseconds, inter-filament coupling loss can have a significant impact on a magnet discharge. Quantitative studies of the effects of transitory loss on the magnet's differential inductance and coil resistance allow improved simulations of quench protection discharges [8], [13], [14]. Accurate modeling of transitory losses are mandatory in order to satisfactorily simulate magnet discharges using the CLIQ (Coupling-Loss Induced Quench) method [15]–[17].

A modeling technique named LEDET (Lumped-Element Dynamic Electro-Thermal) was recently proposed, which is based on the representation of coupling-loss effects by means of an equivalent network of lumped-elements [7], [15]. The LEDET method is applied to efficiently simulate the complex electro-magnetic and thermal transient occurring during a magnet discharge and assess the impact of inter-filament coupling loss on the quench protection performance.

## II. Inter-Filament Coupling Loss

Superconducting wires and strands are composed of superconducting filaments embedded in a matrix of stabilizer material, as shown in the example in Fig. 1. When a varying magnetic field $dB_\mathrm{a}/dt$ [$\mathrm{Ts}^{-1}$] is applied to a superconducting wire, a magnetic field $B_\mathrm{if}$ [T] is induced, which opposes the applied magnetic-field change [1]–[3], [19]. The resulting total magnetic field is the sum of the applied and induced magnetic fields, $B_\mathrm{t}$=$B_\mathrm{a}$+$B_\mathrm{if}$. The induced field is generated by local coupling currents between superconducting filaments, which flow through the resistive wire matrix and develop ohmic loss.

In the case of multiple strands composing a cable, coupling currents through strand contact resistances also develop during transients [3].

The inter-filament coupling currents develop with a characteristic time constant,

$$\tau_{\rm if} = \frac{\mu_0}{2}\left(\frac{l_{\rm f}}{2\pi}\right)^2 \frac{1}{\rho_{\rm eff}}, \quad (1)$$

with $l_{\rm f}$ [m] the filament twist-pitch, $\rho_{\rm eff}$ [$\Omega$m] the effective transverse resistivity of the strand matrix, and $\mu_0{=}4\pi 10^{-7}$ TmA$^{-1}$ the magnetic permeability of vacuum [3], [4]. The effective transverse resistivity can be expressed as the product between the matrix resistivity $\rho_{\rm m}$ [$\Omega$m], determined by its residual resistivity ratio (RRR) and magneto-resistivity, and a parameter $f_{\rm eff}$ depending on the superconductor fraction in the matrix, on the interface resistance between the filaments and the matrix, and on the position of the filaments in the wire cross-section [20]–[22]. In practical round wires, the superconducting filaments are often arranged in an annular region (see $r_{\rm in}{\le}r{\le}r_{\rm fil}$ in Fig. 1), hence forming an inner core and an outer shell of stabilizer [23]. In the case of a round wire of radius $r_{\rm s}$ [m], $f_{\rm eff}$ can be expressed as [24], [25]

$$f_{\rm eff} = \left[\alpha_{\rm in} + \frac{\rho_{\rm m}}{\rho_{\rm eff,fil}}\left(\alpha_{\rm fil}-\alpha_{\rm in}\right) + \alpha_{\rm fil}\frac{1-\alpha_{\rm fil}}{1+\alpha_{\rm fil}}\right]^{-1}, \quad (2)$$

where $\alpha_{\rm in}{=}(r_{\rm in}/r_{\rm s})^2$ and $\alpha_{\rm fil}{=}(r_{\rm fil}/r_{\rm s})^2$ are dimensionless geometric parameters, and $\rho_{\rm eff,fil}$ [$\Omega$m] is the effective transverse resistivity in the annular region. [1] The value of $\rho_{\rm eff,fil}/\rho_{\rm m}$ is comprised between the values

$$\frac{1-f_{\rm sc,fil}}{1+f_{\rm sc,fil}}, \text{ and } \frac{1+f_{\rm sc,fil}}{1-f_{\rm sc,fil}}, \quad (3)$$

with $f_{\rm sc,fil}$ the fraction of superconductor in the annular filamentary region, in the case the superconducting filaments do or do not contribute to the transverse conduction, respectively [20]–[22]. The former case occurs for small interface resistance between the filaments and the matrix; whereas the latter occurs if the interface resistance is large.

During transients with constant applied magnetic-field change, the power generated per unit of wire volume is [3]

$$P'''_{\rm if} = \left(\frac{l_{\rm f}}{2\pi}\right)^2 \frac{1}{\rho_{\rm eff}}\left(\frac{dB_{\rm t}}{dt}\right)^2 = \frac{2}{\mu_0}\tau_{\rm if}\left(\frac{dB_{\rm t}}{dt}\right)^2. \quad (4)$$

During fast transients, i.e. when the magnetic field changes rapidly with respect to $\tau_{\rm if}$, a more detailed characterization of $P'''_{\rm if}$ is required [7], [25]–[27].

## III. LEDET Model

The LEDET method allows modeling the electro-magnetic and thermal transients in a superconducting magnet by means of networks of lumped-elements [7], [15]. This approach was used in a stand-alone application with the same name and in the TALES software [7], [15], [28], [29], and has been routinely validated against experimental results [15], [30]–[32].

[1] This formula corrects the one proposed in [7], [15].

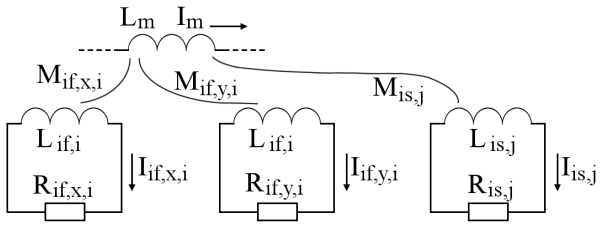


Fig. 2. LEDET technique [7], [15]. Schematic of the RL dissipative loops mutually coupled with the magnet self-inductance $L_{\rm m}$, modeling the inter-filament coupling effects in one strand volume ($R_{\rm if,x,i}$, $R_{\rm if,y,i}$, $L_{\rm if,i}$, $M_{\rm if,x,i}$, $M_{\rm if,y,i}$) and the inter-strand coupling effects in one cable volume ($R_{\rm is,j}$, $L_{\rm is,j}$, $M_{\rm is,j}$).

The model is composed of three sub-networks simulating the coupled effects of electrical transients in the the magnet circuit, thermal transients in the coil turns, and coupling effects in the cable. The dynamics of coupling currents in different volumes of conductor are represented with arrays of RL dissipative loops coupled with the magnet self-inductance, as shown in Fig. 2.

In general, any coupling-current mechanism occurring in a volume $V_{\rm cc}$ [m$^3$] is characterized by a loss $P_{\rm cc}$ [W] and an equivalent coupling-current $I_{\rm cc}$ [A], described by the following two relations:

$$\begin{cases} P_{\rm cc} = \beta_{\rm cc} V_{\rm cc}\left(\dfrac{dB_{\rm cc}}{dt}\right)^2 & [\rm W] \\ I_{\rm cc} = -\gamma_{\rm cc}\dfrac{dB_{\rm cc}}{dt}, & [\rm A] \end{cases} \quad (5)$$

plus a characteristic time constant, $\tau_{\rm cc}$ [s], with $dB_{\rm cc}/dt$ [Ts$^{-1}$] the resulting total magnetic-field change, and $\beta_{\rm cc}$ [m$\Omega^{-1}$] and $\gamma_{\rm cc}$ [m$^2\Omega^{-1}$] characteristic parameters depending on the loss mechanism. The dynamics between the coupling current and the magnet transport current is described by the following equation [7], [15]:

$$-R_{\rm cc}I_{\rm cc} = M_{\rm cc}dI_{\rm m}/dt + L_{\rm cc}dI_{\rm cc}/dt, \quad [\rm V] \quad (6)$$

where the equivalent resistance $R_{\rm cc}$, self-inductance $L_{\rm cc}$, and mutual inductances $M_{\rm cc}$ of the generic coupling-current loop are defined as:

$$\begin{cases} R_{\rm cc} = \dfrac{P_{\rm cc}}{I_{\rm cc}^2} = \dfrac{\beta_{\rm cc}V_{\rm cc}}{\gamma_{\rm cc}^2} & [\Omega] \\ L_{\rm cc} = \tau_{\rm cc}R_{\rm cc} = \dfrac{\tau_{\rm cc}\beta_{\rm cc}V_{\rm cc}}{\gamma_{\rm cc}^2} & [\rm H] \\ M_{\rm cc} = \dfrac{\beta_{\rm cc}V_{\rm cc}}{\gamma_{\rm cc}}f_{\rm m,cc} & [\rm H] \end{cases} \quad (7)$$

with $f_{\rm m,cc}$ [TA$^{-1}$] the magnetic parameters defining the applied magnetic field $B_{\rm a}$ generated by the current $I_{\rm m}$ in the volume $V_{\rm cc}$. The parameters $f_{\rm m,cc}$ are calculated by means of dedicated software, such as ROXIE [33] or SOLENO [34]. In first approximation, they are purely geometric. The parameters $R_{\rm cc}$, $L_{\rm cc}$, and $M_{\rm cc}$ have been analytically calculated for the cases of inter-filament coupling currents in round wires and inter-strand coupling currents in Rutherford cables [7], [15].

The dynamics defined by (6) is reproduced by an equivalent RL loop mutually coupled with the magnet self-inductance. When the magnet current changes, the local current $I_{\rm cc}$ arises

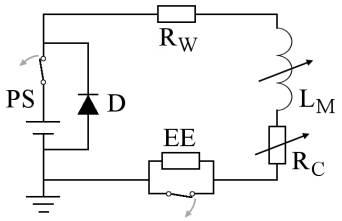


Fig. 3. Simplified schematic of a quench protection circuit including a magnet ($\mathrm{L_M}$), power supply (PS), by-pass diode (D), room-temperature resistance ($\mathrm{R_W}$), and energy-extraction system (EE).

and the energy dissipated in $R_{\mathrm{cc}}$ equals the coupling loss generated in the volume $V_{\mathrm{cc}}$. For sufficiently long magnets, a 2D approximation is satisfactory. The coupling effects in a coil whose cross-section includes $N_{\mathrm{s}}$ strands and $N_{\mathrm{c}}$ cables can be reproduced by $2N_{\mathrm{s}}$ loops simulating inter-filament coupling currents developed in the strands in the two directions $x$ and $y$ perpendicular to the transport current (see $R_{\mathrm{if,x,i}}$, $R_{\mathrm{if,y,i}}$, $L_{\mathrm{if,i}}$, $M_{\mathrm{if,x,i}}$, $M_{\mathrm{if,y,i}}$ in Fig. 2), and by $N_{\mathrm{c}}$ loops simulating inter-strand coupling currents in the cables (see $R_{\mathrm{is,j}}$, $L_{\mathrm{is,j}}$, $M_{\mathrm{is,j}}$ in Fig. 2). The effects of additional coupling mechanisms can be simulated by including in the model other RL loops similar to those described in this section, described by characteristic $R_{\mathrm{cc}}$, $L_{\mathrm{cc}}$, and $M_{\mathrm{cc}}$.

## IV. Magnet Quench Protection

Several mechanisms can lead to a transition to the normal state of a part of a superconducting coil, i.e. a quench [4], [35]–[38]. The goal of the magnet protection system is assuring a safe discharge of the magnet's stored energy after such an event [38]–[41]. In Fig. 3, a simple example of quench protection circuit is shown, including a magnet ($\mathrm{L_M}$), a power supply (PS) with its by-pass diode (D), the circuit room-temperature resistance ($\mathrm{R_W}$), usually due to the current leads, and an energy-extraction system (EE). After quench, an electrical resistance $R_{\mathrm{c}}$ [Ω] builds up across the coil sections that have transitioned to the normal state. Upon quench detection, the power supply is switched off and the energy-extraction switch is opened, thus resulting in a discharge of the magnet transport current with varying ramp rate,

$$dI_{\mathrm{m}}(t)/dt = -I_{\mathrm{m}}(t)\left[R_{\mathrm{EE}} + R_{\mathrm{w}} + R_{\mathrm{c}}(t)\right]/L_{\mathrm{d}}(t), \qquad (8)$$

where $R_{\mathrm{EE}}$ and $R_{\mathrm{w}}$ [Ω] are the resistances of the energy-extraction resistor and of the circuit's warm elements, respectively, and where the voltage drop across D, usually much smaller than the other terms, is neglected. Note that both $R_{\mathrm{c}}$ and $L_{\mathrm{d}}$ are time-dependent.

The effect of inter-filament coupling loss on the performance of different protection systems is assessed, using as a case study the 150 mm aperture, two-layer, 12 T, $Nb_3Sn$ quadrupole magnet for the High Luminosity LHC (HL-LHC) upgrade [42]–[45].

### A. Energy Extraction System

An energy-extraction system (see Fig. 3) features a switch that is opened after quench detection to divert the magnet current to a resistor, in which part of the magnet energy is deposited.

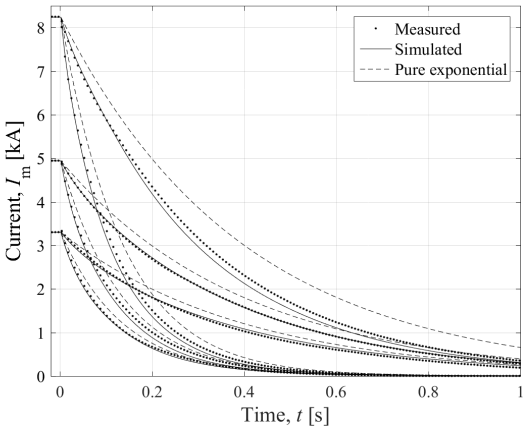


Fig. 4. Comparison between measured and simulated currents during the discharges of the HL-LHC quadrupole model magnet at currents ranging from 20 to 50% of the nominal current, obtained by triggering an energy-extraction system ($R_{\mathrm{EE}}$=30 and 90 mΩ), versus time.

A 1.2 m long model for the HL-LHC quadrupole magnet was tested at FNAL in the circuit configuration shown in Fig. 3 [46]. The magnet is discharged at initial currents $I_0$ [A] ranging between 20 and 50% of the 16.5 kA nominal current by means of an energy-extraction system with resistance $R_{\mathrm{EE}}$=30 or 90 mΩ. In absence of transitory losses and quench, the magnet differential inductance would equal the nominal value of $L_0$=12.2 mH and the coil resistance would be nil during the entire discharge. Thus, the transport current would decay exponentially, following (8) with $R_{\mathrm{c}}$=0 and $L_{\mathrm{d}}$=$L_0$.

However, inter-filament and inter-strand coupling currents and other transitory losses reduce $L_{\mathrm{d}}$ and can initiate a transition to the normal state of parts of the coil, hence inducing a non-zero $R_{\mathrm{c}}$. As a result, the magnet discharges are significantly faster than pure exponential decays, as shown in Fig. 4. The current discharges are simulated with the LEDET model described in Section III. In the absence of experimental data for $f_{\mathrm{eff}}$ of the strand used in this magnet, it is found that a value of 0.75 provides the best agreement with the measured curves. As later explained in Section IV-C, this value is well within the range of values expected from the wire specifications.

The faster discharge is mainly due to the decrease of $L_{\mathrm{d}}$, especially in the first tens of milliseconds just after triggering the energy extraction. This conclusion is reached by calculating the experimental magnet differential inductance and the coil resistance. The same quantities are computed with the LEDET model, providing simulated time-dependent values, $L_{\mathrm{d}}^*$ [H] and $R_{\mathrm{c}}^*$ [Ω], which can be used to refine the calculation of $L_{\mathrm{d}}$ and $R_{\mathrm{c}}$ from magnet current-voltage measurements.

The voltage across the magnet is the sum of the inductive and resistive contributions,

$$U_{\mathrm{M}}(t) = L_{\mathrm{d}}(t)dI_{\mathrm{m}}(t)/dt + R_{\mathrm{c}}(t)I_{\mathrm{m}}(t). \qquad (9)$$

In the approximation of $R_{\mathrm{c}}$≈0, the differential inductance

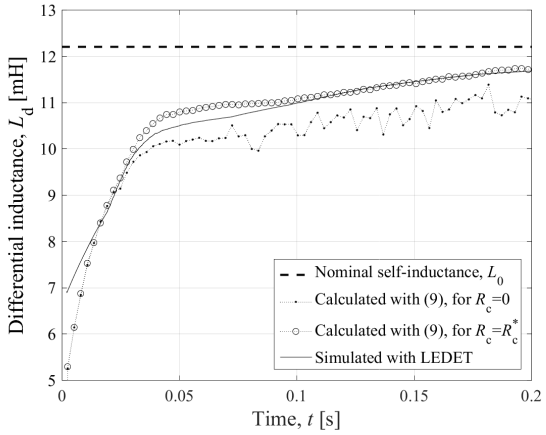


Fig. 5. Comparison between experimental and simulated differential inductances during the discharge of the HL-LHC quadrupole model magnet at $I_0$=8.24 kA with a 90 mΩ energy-extraction system, versus time.

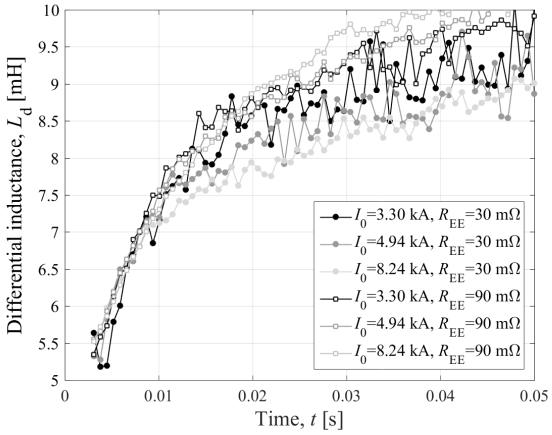


Fig. 6. Calculated differential inductances during the discharges of the HL-LHC quadrupole model magnet at currents ranging from 20 to 50% of the nominal current, obtained by triggering an energy-extraction system ($R_{EE}$=30 and 90 mΩ), versus time.

is calculated as $U_M/(dI_m/dt)$. However, the coil resistance simulated with LEDET can be used to improve the accuracy of this estimation, as in $L_d \approx (U_M - R_c^* I_m)/(dI_m/dt)$. In Fig. 5, the experimental and simulated differential inductances during a 90 mΩ energy-extraction at 50% nominal current are compared.

The reduction of about 50% of the experimental $L_d$ just after triggering, reproduced quite well by the model, is due to two main contributions. First, $L_d$ is reduced by an amount $\Delta L_{iron}$ [H] due to saturation of the iron-yoke surrounding the magnet, which depends on the current level. Second, $L_d$ is further decreased due to inter-filament and inter-strand coupling currents, whose effects decay with their characteristic time constants. In the present example, during the first 50 ms of discharge $L_d$ rapidly increases back towards the nominal self-inductance $L_0$ due to the decay of the coupling currents when $dI_m/dt$ is decreasing. The time-scale of the reduction is consistent with the inter-filament coupling-current time constants, estimated between 10 and 70 ms in the high- and low-field strands, respectively. The even higher experimental $L_d$ reduction in the first milliseconds after triggering is likely due to additional transitory loss mechanisms not included in the model, such as hysteresis in the superconductor and eddy currents in the magnet's copper wedges.

Interestingly, for a given magnet design the reduction of $L_d$ due to coupling currents just after triggering is almost independent of the initial current level and ramp-rate, filament twist-pitch and strand effective transverse resistivity. Instead, it is determined mainly by the strand diameter and by the positions of the strands, which determine the magnetic parameters $f_{m,cc}$ defined in (7). The only dependence on the magnet current is due to the indirect effect of the iron-yoke saturation, which slightly affects the parameters $f_{m,cc}$. The experimental differential inductances observed during the tests, shown in Fig. 6, exhibit very similar reductions, even if the ramp-rates in the tests differ by about one order of magnitude.

This result is explained by considering the differential inductance predicted by the model. From Faraday's law of induction, $L_d$ can be expressed as the ratio between the magnet inductive voltage and its current change, $L_d = U_{ind}/(dI_m/dt)$. In turn, $U_{ind}$ is calculated as the sum of the contribution of the magnet self-inductance and the mutual coupling with the $2N_s+N_c$ equivalent loops described in Section III,

$$\begin{aligned} U_{ind} = {} & [L_0 - \Delta L_{iron}(I_m)] \frac{dI_m}{dt} \\ & + \sum_{i=1}^{N_s} \left( M_{if,x,i} \frac{dI_{if,x,i}}{dt} + M_{if,y,i} \frac{dI_{if,y,i}}{dt} \right) \\ & + \sum_{j=1}^{N_c} M_{is,j} \frac{dI_{is,j}}{dt}, \end{aligned} \tag{10}$$

where $\Delta L_{iron}$ [H] is the reduction of $L_d$ due to the saturation of the iron yoke surrounding the coil. Note that the mutual coupling components reduce $U_{ind}$ when the coupling currents start developing. Solving (6) for each loop, substituting into (10), and dividing by $dI_m/dt$ yields

$$\begin{aligned} L_d = {} & L_0 - \Delta L_{iron}(I_m) \\ & - \sum_{i=1}^{N_s} \frac{M_{if,x,i}^2 + M_{if,y,i}^2}{L_{if,i}} - \sum_{j=1}^{N_c} \frac{M_{is,j}^2}{L_{is,j}} \\ & - \sum_{i=1}^{N_s} \left( M_{if,x,i} \frac{I_{if,x,i}/\tau_{if,x,i}}{dI_m/dt} + M_{if,y,i} \frac{I_{if,y,i}/\tau_{if,y,i}}{dI_m/dt} \right) \\ & - \sum_{j=1}^{N_c} M_{is,j} \frac{I_{is,j}/\tau_{is,j}}{dI_m/dt}. \end{aligned} \tag{11}$$

At the moment of the EE triggering, all coupling currents are zero ($I_{if,x,i}$=$I_{if,y,i}$=$I_{is,j}$=0) and therefore the two latter sums in (11) are nil. Thus, the initial value of $L_d$ only depends on $\Delta L_{iron}$ and the parameters $L_{if,i}$, $L_{is,j}$, $M_{if,x,i}$, $M_{if,y,i}$, and $M_{is,j}$. For this magnet design, the estimated contributions to the initial $L_d$ reduction due to inter-filament and inter-strand coupling currents, equal to the first two sums in (11), are 22

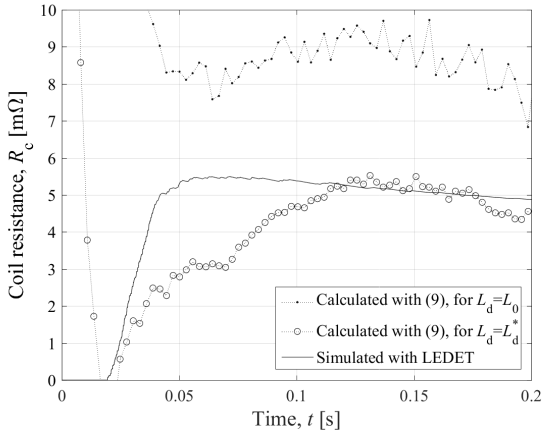


Fig. 7. Comparison between experimental and simulated coil resistance during the discharge of the HL-LHC quadrupole model magnet at $I_0$=8.24 kA with a 90 mΩ energy-extraction system, versus time.

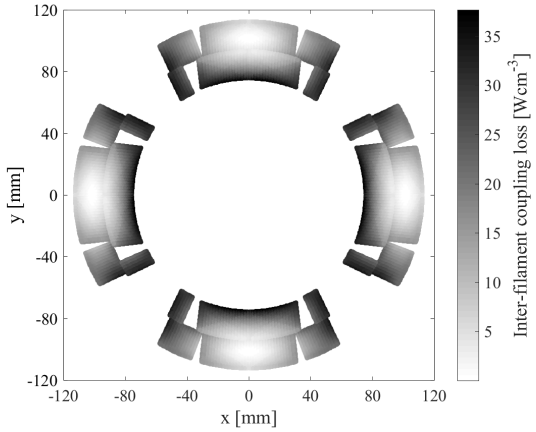


Fig. 8. Simulated peak inter-filament coupling loss per unit volume generated in the strands during the discharge of the HL-LHC quadrupole model magnet at $I_0$=8.24 kA with a 90 mΩ energy-extraction system.

and 5% of $L_0$, respectively, whereas $\Delta L_{\rm iron}$ varies from 6 to 13% of $L_0$ between 20 and 50% of nominal current.

While the initial reduction of $L_{\rm d}$ can be calculated analytically with good approximation, the speed with which $L_{\rm d}$ recovers towards $L_0$ is influenced by the values of the coupling-current time constants. The time constants $\tau_{\rm if}$ in the strands depend on the effective transverse resistivity, which in turn is influenced by $f_{\rm eff}$ and by the current level due to magneto-resistivity. Furthermore, if a transition to the normal state is induced by the transitory losses, the matrix resistivity increases abruptly due to ohmic heating, which accelerates the coupling-current decay process.

If the coil resistance during a discharge was calculated simply assuming $L_{\rm d}{\approx}L_0$ in (9), one would obtain $R_{\rm c}{\approx}(U_{\rm M}{-}L_0 dI_{\rm m}/dt)/I_{\rm m}$. This approximation can lead to large errors, especially during the first tens of milliseconds of discharge. By substituting in (9) the time-dependent differential inductance simulated with LEDET, one can obtain a more accurate result, $R_{\rm c}{\approx}(U_{\rm M}{-}L_{\rm d}^* dI_{\rm m}/dt)/I_{\rm m}$.

The coil resistance developed during the 90 mΩ energy-extraction at 50% nominal current is plotted in Fig. 7. Without implementing the correction, the experimental $R_{\rm c}$ is overestimated by almost 100%. With the proposed correction, the simulated and experimental $R_{\rm c}$ are in good agreement, with the exception of the time between $t$=40 and 100 ms, when a 3% underestimation of the simulated $L_{\rm d}$ (see Fig. 5) results in an insufficient correction of $R_{\rm c}$.

In many applications, it is of interest to assess which parts of the coil cross-section are subject to the highest deposited loss. In Fig. 8, the distribution of the peak inter-filament coupling loss per unit volume generated in the strands during the discharge presented in Fig. 5 and 7 is shown. Predictably, highest coupling loss is developed in the strands located in the coil's inner layer, where the magnetic-field change is highest, while almost no loss is developed in the mid-plane outer turns, where the magnetic-field change is very small.

### *B. Quench Heaters*

Protecting high current-density, compact, long superconducting coils with an energy-extraction system would require very high voltages to ground, which are beyond safe limits of laboratory and accelerator equipment. Therefore, the quench protection strategy is based on actively transferring the superconductor to the normal state, hence forcing the discharge of the magnet stored energy with the coil resistance. A conventional method to achieve this relies on quench heaters, consisting of thin stainless steel strips in thermal contact with the insulation layer of the coil to protect. Upon quench detection, a current is introduced through the strips and heat is transferred to the coil turns via thermal diffusion.

The validated LEDET model can offer a quantitative estimation of the coupling-loss contribution to the discharge and provide realistic information to assess and optimize the protection system. This constitutes a significant improvement over models neglecting altogether the $L_{\rm d}$ reduction and the transition of parts of the coil to the normal state due to transitory losses, which may result in overly pessimistic results.

The discharge of a full-scale 7.15 m long HL-LHC quadrupole magnet by means of quench heaters attached to the coil's outer layer is simulated. In absence of energy-extraction and given the very little room-temperature circuit resistance, the current is mainly discharged by $R_{\rm c}$. The currents and coil's hot-spot temperature $T_{\rm hot}$ [K] after a quench at nominal current, simulated with and without coupling currents, are compared in Fig. 9. As expected, the presence of coupling currents results in a faster magnet discharge, which in this example reduces $T_{\rm hot}$ by more than 50 K.

The discharge is influenced by the coupling currents only about 50 ms after triggering the protection system. This result can be explained by observing the simulated differential inductance and coil resistance, shown in Fig. 10. As in the case of an EE discharge, $L_{\rm d}$ is greatly reduced by the coupling currents developed immediately after the

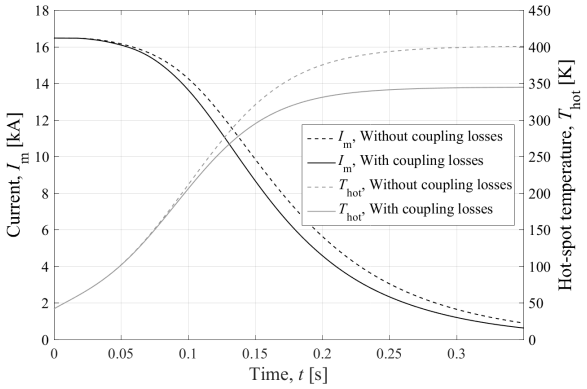


Fig. 9. Effect of coupling currents on the quench-heater induced discharge of the 7.15 m HL-LHC quadrupole model magnet at nominal current. Comparison of currents and hot-spot temperatures simulated with and without coupling-current effects, versus time.

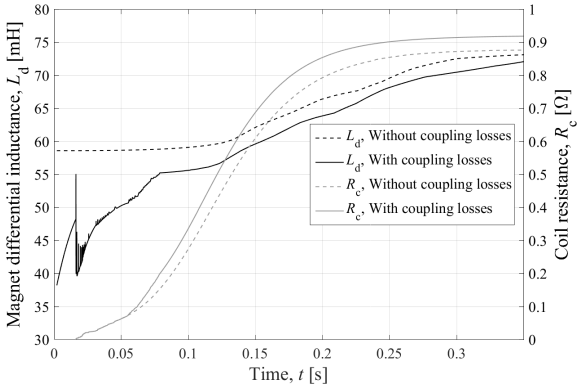


Fig. 10. Effect of coupling currents on the quench-heater induced discharge of the 7.15 m HL-LHC quadrupole model magnet at nominal current. Comparison of magnet differential inductance and coil resistance simulated with and without coupling-current effects, versus time.

power-supply switching-off. Iron-yoke saturation, included in both simulations, reduces $L_{\rm d}$ by 19% with respect to $L_0$=73.4 mH at nominal current, whereas inter-filament and inter-strand coupling losses reduce it by an additional 28%. However, the effects of inter-filament coupling currents decay in a few tens of milliseconds due to their short characteristic time constant and reduce $L_{\rm d}$ mainly when the coil resistance is zero or very small. Inter-strand coupling currents last about ten times longer and reduce $L_{\rm d}$ during the entire discharge, but their contribution is only 4% of $L_0$. Thus, it can be concluded that coupling currents induce a faster discharge mainly due to the more rapid increase of $R_{\rm c}$. In fact, coupling losses generated in the conductor speed up the heating process and result in a faster transition to the normal state, and hence higher $R_{\rm c}$.

### C. CLIQ

A different active quench heating mechanism is based on the CLIQ system [15]–[17], successfully tested on magnets of different geometries, superconductor types, and sizes [30]–[32], [47], [48]. This method consists in introducing

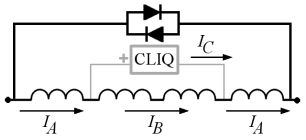


Fig. 11. Simplified electrical scheme of a magnet protected by a CLIQ unit.

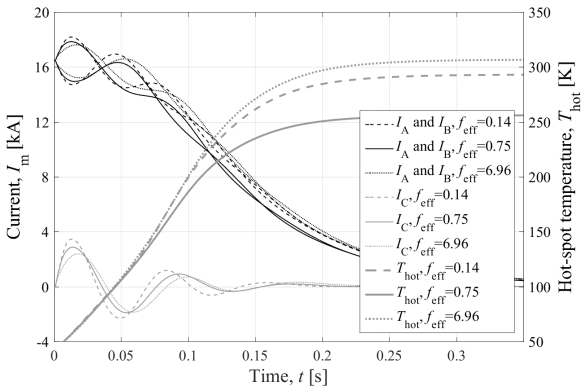


Fig. 12. Effect of effective transverse resistivity on the CLIQ-induced discharge of the 7.15 m HL-LHC quadrupole model magnet at nominal current. Simulated currents and coil's hot-spot temperature versus time, for different values of $f_{\rm eff}$.

oscillating opposite current changes in different coil sections by means of a capacitive discharge through terminals connected to the coil to protect, as shown in the simple scheme in Fig. 11. The oscillating currents $I_{\rm A}$ and $I_{\rm B}$ [A] generate magnetic-field changes, which in turn develop high coupling losses in the superconductor.

For practical magnet self-inductances and CLIQ unit capacitances, the introduced current $I_{\rm C}$ [A] usually oscillates at a frequency between 10 and 100 Hz. In this frequency range, inter-filament coupling loss is generally the most effective means to quickly deposit energy in the coil and transfer it to the normal state due to its short characteristic time constant. Besides, the presence of inter-filament coupling currents reduces significantly the differential inductance.

This section gives a brief overview of the effect of coupling currents on CLIQ performance and the simulation capabilities of the LEDET model. We refer to [15] for a more complete treatise. As a case study, the same HL-LHC full-size magnet described in the previous section, protected by one 1 kV, 40 mF CLIQ unit connected as described in [13], [14], is analyzed here. For the strand used in this magnet, $f_{\rm eff}$ is estimated between 0.14 and 6.96 using (2) and the extremes defined in (3), with $\alpha_{\rm in}$=0.068, $\alpha_{\rm fil}$=0.689, and $f_{\rm sc,fil}$=0.749.

The simulated currents in the coil sections and those introduced by CLIQ are plotted in Fig. 12, for three different values of $f_{\rm eff}$. The lower the effective transverse resistivity, the higher inter-filament coupling currents develop, and hence the more they reduce the differential inductance. Thus, for lower $f_{\rm eff}$ the introduced current oscillates more quickly and reaches a higher peak. On the contrary, the most effective energy deposition is achieved for an intermediate value of $f_{\rm eff}$. As can be observed from (1) and (4), the effective transverse resistivity

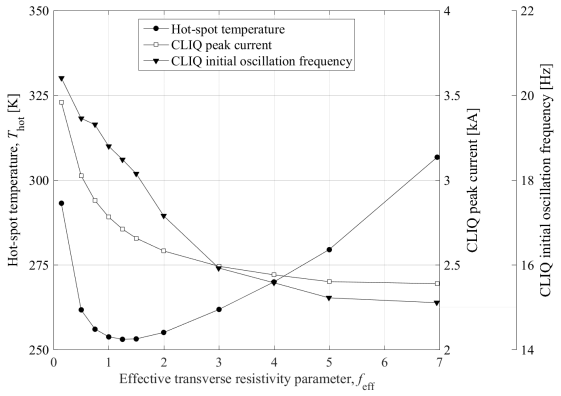


Fig. 13. Effect of effective transverse resistivity on the CLIQ-induced discharge of the 7.15 m HL-LHC quadrupole model magnet at nominal current. Simulated coil's hot-spot temperature and peak value and oscillation frequency of the current introduced by CLIQ, versus $f_{\rm eff}$.

is inversely proportional both to the inter-filament coupling loss and to their characteristic time constant. Thus, in strands with low $\rho_{\rm eff}$ more inter-filament coupling loss is developed, but more slowly, and vice versa. Both cases of minimum and maximum $f_{\rm eff}$ result in higher hot-spot temperature than the case $f_{\rm eff}$=0.75, as shown in Fig. 12.

The range of $f_{\rm eff}$ within which good CLIQ performance is achieved is relatively wide. This result can be observed in Fig. 13, where the simulated hot-spot temperatures are plotted as a function of $f_{\rm eff}$. For $f_{\rm eff}$ in the range 0.5 to 3, $T_{\rm hot}$ varies less than 10 K. For the minimum and maximum estimated $f_{\rm eff}$, the increase of $T_{\rm hot}$ is about 50 K.

The initial frequency $f_{\rm CLIQ}$ [Hz] and peak value of the oscillating current $I_{\rm CLIQ,peak}$ [A] are affected more significantly by $f_{\rm eff}$. Both parameters are higher than the values calculated in absence of transitory losses, $f_{\rm CLIQ}$=10.2 Hz and $I_{\rm CLIQ,peak}$=2.3 kA.

## V. Summary and Outlook

Transitory losses developed during the discharge of a superconducting magnet can significantly affect its protection against the effects of a quench. Inter-filament coupling currents often influence the discharge dynamics due to their short time constant, usually of the order of a few milliseconds or tens of milliseconds. These currents reduce the magnet differential inductance due to the local magnetic-field changes they induce in the conductor. Furthermore, the coupling losses generated in the conductor increase its temperature and can cause a transition to the normal state during the discharge. The influence of inter-strand coupling currents is usually more limited due to the longer time-constant characterizing their development.

The model developed with the LEDET technique provides a quantitative estimation of the coupling current effects. The method relies on a network of lumped-elements that reproduces the coupling-current dynamics and can be solved simultaneously to conventional electrical and thermal networks. After its validation, the model is used to study the effects of inter-filament and inter-strand coupling currents on different magnet quench protection systems.

In the case of an energy-extraction system, coupling currents are often relevant for the system dynamics. Immediately after triggering the extraction, coupling currents reduce the magnet differential inductance by an amount that can be reliably estimated with the LEDET technique. Moreover, the loss developed in the conductor can cause a transition to the normal state, which further increases the discharge velocity.

In the case of a protection system based on quench heaters, the reduction of magnet differential inductance due to coupling currents usually does not improve the quench protection performance significantly. In fact, the differential inductance reduction occurs at a time when the coil resistance is nil or very small, hence the effective current change is very limited. However, coupling losses contribute to the heating of the conductor and speed up its transition to the normal state, which in many practical cases results in a significant reduction of the coil's hot-spot temperature at the end of the discharge.

In the case of a system relying on CLIQ, the transition to the normal state is induced by utilizing coupling losses as an heating mechanism. The quench protection performance is mostly independent of the effective transverse resistivity. In fact, in lower-resistivity wires higher inter-filament coupling currents are developed, but with a higher characteristic time constant, and the two effects compensate each other. On the contrary, the oscillating current introduced by CLIQ is influenced significantly by the effective transverse resistivity. Coils with lower-resistivity wires develop higher inter-filament coupling currents, which results in a higher inductance reduction, and hence higher oscillating frequency and peak introduced current.

The LEDET model can be used as an efficient tool to simulate the complex electro-magnetic and thermal transient occurring during a magnet discharge and assess the impact of inter-filament and inter-strand coupling losses on the quench protection performance.

## References

[1] G. H. Morgan, "Theoretical behavior of twisted multicore superconducting wire in a time-varying uniform magnetic field," *Journal of Applied Physics*, vol. 41, no. 9, 1970.

[2] W. J. Carr, "AC loss in a twisted filamentary superconducting wire," *Journal of Applied Physics*, vol. 45, no. 2, 1974.

[3] A. P. Verweij, "Electrodynamics of superconducting cables in accelerator magnets," Ph.D. dissertation, Twente U., Twente, 1995, presented on 15 Sep 1995. [Online]. Available: https://cds.cern.ch/record/292595

[4] M. Wilson, *Superconducting Magnets*, ser. Monographs on Cryogenics. Clarendon Press, 1983.

[5] E. Ravaioli, K. Dahlerup-Petersen, F. Formenti, J. Steckert, H. Thiesen, and A. Verweij, "Modeling of the voltage waves in the lhc main dipole circuits," *IEEE Transactions on Applied Superconductivity*, vol. 22, no. 3, pp. 9 002 704–9 002 704, June 2012.

[6] E. Ravaioli, K. Dahlerup-Petersen, F. Formenti, V. Montabonnet, M. Pojer, R. Schmidt, A. Siemko, M. S. Camillocci, J. Steckert, H. Thiesen, and A. Verweij, "Impact of the voltage transients after a fast power abort on the quench detection system in the lhc main dipole chain," *IEEE Transactions on Applied Superconductivity*, vol. 22, no. 3, pp. 9 002 504–9 002 504, June 2012.

[7] E. Ravaioli, B. Auchmann, M. Maciejewski, H. ten Kate, and A. Verweij, "Lumped-element dynamic electro-thermal model of a superconducting magnet," *Cryogenics*, pp. –, 2016. [Online]. Available: http://www.sciencedirect.com/science/article/pii/S0011227516300832

[8] V. Marinozzi, M. Sorbi, G. Manfreda, F. Bellina, H. Bajas, and G. Chlachidze, "Effect of coupling currents on the dynamic inductance during fast transient in superconducting magnets," *Phys. Rev. ST Accel. Beams*, vol. 18, p. 032401, Mar 2015. [Online]. Available: http://link.aps.org/doi/10.1103/PhysRevSTAB.18.032401

[9] M. Green, "Quench back in thin superconducting solenoid magnets," *Cryogenics*, vol. 24, no. 1, pp. 3–10, 1984. [Online]. Available: http://www.sciencedirect.com/science/article/pii/0011227584900493

[10] M.A. Green, "The role of quench back in quench protection of a superconducting solenoid," *Cryogenics*, vol. 24, no. 12, pp. 659–668, 1984. [Online]. Available: http://www.sciencedirect.com/science/article/pii/0011227584900341

[11] K. Takeuchi, Y. Kang, H. Hashizume, and Y. Iwasa, "Interfilament coupling loss for protection of superconducting multicoil magnets," *Cryogenics*, vol. 38, no. 4, pp. 367–376, 1998. [Online]. Available: http://www.sciencedirect.com/science/article/pii/S0011227598000034

[12] F. Sonnemann and R. Schmidt, "Quench simulations for superconducting elements in the LHC accelerator," *Cryogenics*, vol. 40, no. 810, pp. 519–529, 2000, 4th Workshop on Computation of Thermal Hydraulic Transients in Superconductors. [Online]. Available: http://www.sciencedirect.com/science/article/pii/S001122750100008X

[13] E. Ravaioli, B. Auchmann, V. I. Datskov, J. Blomberg Ghini, K. Dahlerup-Petersen, A. M. Fernandez Navarro, G. Kirby, M. Maciejewski, F. Rodriguez-Mateos, H. H. J. ten Kate, and A. P. Verweij, "Advanced quench protection for the $Nb_3Sn$ quadrupoles for the High Luminosity LHC," *IEEE Transactions on Applied Superconductivity*, vol. 26, no. 3, pp. 1–6, April 2016.

[14] E. Ravaioli, G. Ambrosio, B. Auchmann, P. Ferracin, M. Maciejewski, F. Rodriguez-Mateos, G. Sabbi, E. Todesco, and A. Verweij, "Quench protection system optimization for the High Luminosity LHC $Nb_3Sn$ quadrupoles," *IEEE Transactions on Applied Superconductivity*, 2017.

[15] E. Ravaioli, "CLIQ," Ph.D. dissertation, Enschede, 2015, presented on 19 June 2015. [Online]. Available: http://doc.utwente.nl/96069/

[16] V. Datskov, G. Kirby, and E. Ravaioli, "AC-current induced quench protection system," Patent EP13 174 323.9, June 28, 2013.

[17] E. Ravaioli, V. I. Datskov, C. Giloux, G. Kirby, H. H. J. ten Kate, and A. P. Verweij, "New, Coupling Loss Induced, Quench protection system for superconducting accelerator magnets," *IEEE Transactions on Applied Superconductivity*, vol. 24, no. 3, pp. 1–5, June 2014.

[18] O. Brüning, P. Collier, P. Lebrun, S. Myers, R. Ostojic, J. Poole, and P. Proudlock, *LHC Design Report*. Geneva: CERN, 2004. [Online]. Available: https://cds.cern.ch/record/782076

[19] S. Russenschuck, *Field computation for accelerator magnets: Analytical and numerical methods for electromagnetic design and optimization*. Weinheim: Wiley-VCH, 2010. [Online]. Available: http://eu.wiley.com/WileyCDA/WileyTitle/productCd-3527407693.html

[20] W. J. Carr, M. S. Walker, and J. H. Murphy, "Alternating field loss in a multifilament superconducting wire for weak ac fields superposed on a constant bias," *Journal of Applied Physics*, vol. 46, no. 9, 1975.

[21] M. Walker, J. Murphy, and W. Carr, "Alternating field losses in mixed matrix multifilament superconductors," *IEEE Transactions on Magnetics*, vol. 11, no. 2, pp. 309–312, Mar 1975.

[22] M. Walker, W. Carr, and J. Murphy, "Loss behavior in twisted filamentary superconductors," *IEEE Transactions on Magnetics*, vol. 11, no. 5, pp. 1475–1477, Sep 1975.

[23] C. Zhou, Y. Miyoshi, E. P. A. van Lanen, M. Dhall, and A. Nijhuis, "Inter-filament resistance, effective transverse resistivity and coupling loss in superconducting multi-filamentary nbti and $Nb_3Sn$ strands," *Superconductor Science and Technology*, vol. 25, no. 6, p. 065018, 2012. [Online]. Available: http://stacks.iop.org/0953-2048/25/i=6/a=065018

[24] D. Ciazynski, "Distributions de courant et pertes à l'intérieur d'un composite multifilamentaire supraconducteur soumis à un champ magnétique variable," Ph.D. dissertation, Paris, France, 1985.

[25] A. Louzguiti, L. Zani, D. Ciazynski, B. Turck, and F. Topin, "Development of an analytical-oriented extensive model for AC coupling losses in multilayer superconducting composites," *IEEE Transactions on Applied Superconductivity*, vol. 26, no. 3, pp. 1–5, April 2016.

[26] B. Turck, "Coupling losses in various outer normal layers surrounding the filament bundle of a superconducting composite," *Journal of Applied Physics*, vol. 50, no. 8, 1979.

[27] B. Turck, "Effect of the respective positions of filament bundles and stabilizing copper on coupling losses in superconducting composites," *Cryogenics*, vol. 22, no. 9, pp. 466–468, 1982. [Online]. Available: http://www.sciencedirect.com/science/article/pii/001122758290131X

[28] M. Maciejewski, "Automated Object-Oriented Simulation Framework for Modelling of Superconducting Magnets at CERN," Master's thesis, Łódź, Tech. U., 2014-09-07. [Online]. Available: http://inspirehep.net/record/1381303/files/CERN-THESIS-2014-317.pdf

[29] M. Maciejewski, E. Ravaioli, B. Auchmann, A. Verweij, and A. Bartoszewicz, "Automated lumped-element simulation framework for modelling of transient effects in superconducting magnets," in *Methods and Models in Automation and Robotics (MMAR), 2015 20th International Conference on*, Aug 2015, pp. 840–845.

[30] E. Ravaioli, H. Bajas, V. I. Datskov, V. Desbiolles, J. Feuvrier, G. Kirby, M. Maciejewski, G. Sabbi, H. H. J. ten Kate, and A. P. Verweij, "Protecting a full-scale $Nb_3Sn$ magnet with CLIQ, the new Coupling-Loss-Induced Quench system," *IEEE Transactions on Applied Superconductivity*, vol. 25, no. 3, pp. 1–5, June 2015.

[31] E. Ravaioli, H. Bajas, V. I. Datskov, V. Desbiolles, J. Feuvrier, G. Kirby, M. Maciejewski, H. H. J. ten Kate, A. P. Verweij, and G. Willering, "First implementation of the CLIQ quench protection system on a full-scale accelerator quadrupole magnet," *IEEE Transactions on Applied Superconductivity*, vol. 26, no. 3, pp. 1–5, April 2016.

[32] E. Ravaioli, V. I. Datskov, G. Dib, A. M. Fernandez Navarro, G. Kirby, M. Maciejewski, H. H. J. ten Kate, A. P. Verweij, and G. Willering, "First implementation of the CLIQ quench protection system on a 14-m-long full-scale LHC dipole magnet," *IEEE Transactions on Applied Superconductivity*, vol. 26, no. 4, pp. 1–5, June 2016.

[33] S. Russenschuck, *ROXIE : Routine for the Optimization of Magnet X-Sections, Inverse Field Calculation and Coil End Design*. CERN Geneva, 1999.

[34] SOLENO. A high-precision magnetic field, inductances and forces calculation code for air-core systems of multi-solenoids developed by the applied superconductivity applications group at the University of Twente, Enschede, the Netherlands.

[35] Y. Iwasa, *Case studies in superconducting magnets: design and operational issues; 2nd ed.* Berlin: Springer, 2009. [Online]. Available: https://cds.cern.ch/record/1179850

[36] B. Seeber, *Handbook of Applied Superconductivity*. CRC Press, 1998, no. v. 2.

[37] P. Lee, *Engineering Superconductivity*. Wiley, 2001.

[38] L. Bottura, "Magnet Quench 101," no. arXiv:1401.3927, p. 9 p, Jan 2014, comments: 9 pages, Contribution to WAMSDO 2013: Workshop on Accelerator Magnet, Superconductor, Design and Optimization; 15 - 16 Jan 2013, CERN, Geneva, Switzerland. [Online]. Available: http://cds.cern.ch/record/1643429

[39] B. J. Maddock and G. B. James, "Protection and stabilisation of large superconducting coils," *Electrical Engineers, Proceedings of the Institution of*, vol. 115, no. 4, pp. 543–547, April 1968.

[40] J. H. Schultz, "Protection of superconducting magnets," *IEEE Transactions on Applied Superconductivity*, vol. 12, no. 1, pp. 1390–1395, Mar 2002.

[41] E. Todesco, "Quench limits in the next generation of magnets," no. arXiv:1401.3931, p. 7 p, Jan 2014, comments: 7 pages, Contribution to WAMSDO 2013: Workshop on Accelerator Magnet, Superconductor, Design and Optimization; 15 - 16 Jan 2013, CERN, Geneva, Switzerland. [Online]. Available: http://cds.cern.ch/record/1643430

[42] G. Ambrosio, P. Ferracin, and al., "MQXFS1 Quadrupole Design Report," Tech. Rep., 2016.

[43] P. Ferracin, G. Ambrosio, M. Anerella, F. Borgnolutti, R. Bossert, D. Cheng, D. R. Dietderich, H. Felice, A. Ghosh, A. Godeke, S. Izquierdo Bermudez, P. Fessia, S. Krave, M. Juchno, J. C. Perez, L. Oberli, G. Sabbi, E. Todesco, and M. Yu, "Magnet design of the 150 mm aperture low-$\beta$ quadrupoles for the High Luminosity LHC," *IEEE Transactions on Applied Superconductivity*, vol. 24, no. 3, pp. 1–6, June 2014.

[44] G. Ambrosio, "$Nb_3Sn$ high field magnets for the High Luminosity LHC upgrade project," *IEEE Transactions on Applied Superconductivity*, vol. 25, no. 3, pp. 1–7, June 2015.

[45] E. Todesco, H. Allain, G. Ambrosio, F. Borgnolutti, F. Cerutti, D. Dietderich, L. Esposito, H. Felice, P. Ferracin, G. Sabbi, P. Wanderer, and R. V. Weelderen, "Design studies for the low-beta quadrupoles for the LHC luminosity upgrade," *IEEE Transactions on Applied Superconductivity*, vol. 23, no. 3, pp. 4 002 405–4 002 405, June 2013.

[46] G. Chlachidze, G. Ambrosio, M. Anerella, R. Bossert, E. Cavanna, D. W. Cheng, D. R. Dietderich, J. DiMarco, H. Felice, P. Ferracin, A. K. Ghosh, P. Grosclaude, M. Guinchard, A. R. Hafalia, E. F. Holik, S. I. Bermudez, S. T. Krave, M. Marchevsky, A. Nobrega, D. Orris, H. Pan, J. C. Perez, S. Prestemon, E. Ravaioli, G. Sabbi, T. Salmi, J. Schmalzle, S. E. Stoynev, T. Strauss, C. Sylvester, M. Tartaglia, E. Todesco, G. Vallone, G. Velev, P. Wanderer, X. Wang, and M. Yu, "Performance of the first short model 150-mm-aperture $Nb_3Sn$ quadrupole MQXFS

for the High-Luminosity LHC upgrade," *IEEE Transactions on Applied Superconductivity*, vol. 27, no. 4, pp. 1–5, June 2017.

[47] E. Ravaioli, V. Datskov, A. Dudarev, G. Kirby, K. Sperin, H. ten Kate, and A. Verweij, "First experience with the new Coupling Loss Induced Quench system," *Cryogenics*, vol. 60, pp. 33–43, 2014. [Online]. Available: http://www.sciencedirect.com/science/article/pii/S0011227514000162

[48] E. Ravaioli, V. I. Datskov, G. Kirby, H. H. J. ten Kate, and A. P. Verweij, "A new hybrid protection system for high-field superconducting magnets," *Superconductor Science and Technology*, vol. 27, no. 4, p. 044023, 2014. [Online]. Available: http://stacks.iop.org/0953-2048/27/i=4/a=044023